

# RSC Advances

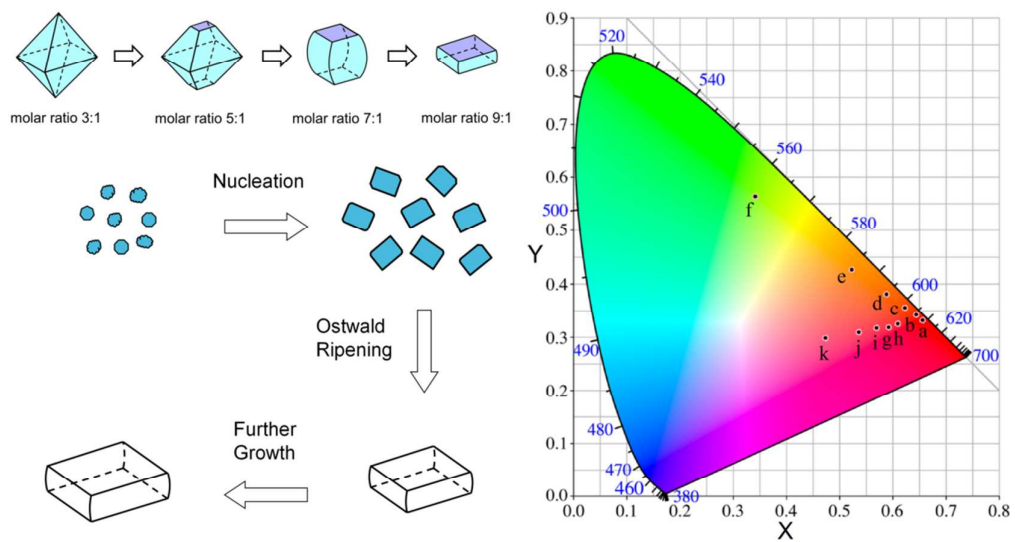


This is an *Accepted Manuscript*, which has been through the Royal Society of Chemistry peer review process and has been accepted for publication.

*Accepted Manuscripts* are published online shortly after acceptance, before technical editing, formatting and proof reading. Using this free service, authors can make their results available to the community, in citable form, before we publish the edited article. This *Accepted Manuscript* will be replaced by the edited, formatted and paginated article as soon as this is available.

You can find more information about *Accepted Manuscripts* in the [Information for Authors](#).

Please note that technical editing may introduce minor changes to the text and/or graphics, which may alter content. The journal's standard [Terms & Conditions](#) and the [Ethical guidelines](#) still apply. In no event shall the Royal Society of Chemistry be held responsible for any errors or omissions in this *Accepted Manuscript* or any consequences arising from the use of any information it contains.



Morphological control, formation mechanism and tunable photoluminescence of NaGd(MoO<sub>4</sub>)<sub>2</sub>: Eu<sup>3+</sup>,Tb<sup>3+</sup> microcrystals synthesized by facile hydrothermal method



## Facile Morphology-controllable Hydrothermal Synthesis and Color Tunable Luminescence Properties of NaGd(MoO<sub>4</sub>)<sub>2</sub>: Eu<sup>3+</sup>, Tb<sup>3+</sup> Microcrystals†

Received 00th January 20xx,  
Accepted 00th January 20xx

DOI: 10.1039/x0xx00000x

www.rsc.org/advances

Anming Li,<sup>a,b</sup> Dekang Xu,<sup>a</sup> Hao Lin,<sup>a</sup> Shenghong Yang,<sup>a</sup> Yuanzhi Shao,<sup>a</sup> Yueli Zhang,<sup>\*a</sup> and Zhenqiang Chen<sup>b</sup>

Well-crystallized and uniform NaGd(MoO<sub>4</sub>)<sub>2</sub> microcrystals with the morphologies of bipyramids, truncated bipyramids, quasi-cubes and tetragonal plates were selectively synthesized via a facile hydrothermal method without any additives under mild conditions. The effects of Na<sub>2</sub>MoO<sub>4</sub>/Gd(NO<sub>3</sub>)<sub>3</sub> molar ratios and pH values of precursor solutions on the phase and morphology of as-synthesized microcrystals were systematically investigated. The molar ratios and pH values played key roles in the selective synthesis of pure phase NaGd(MoO<sub>4</sub>)<sub>2</sub> microcrystals with regular morphology. With increasing Na<sub>2</sub>MoO<sub>4</sub>/Gd(NO<sub>3</sub>)<sub>3</sub> molar ratios in appropriate pH range, the morphology of the products changed from bipyramids, truncated bipyramids, quasi-cubes to tetragonal plates, namely, the morphological truncation degree increased gradually. NaGd(MoO<sub>4</sub>)<sub>2</sub> tetragonal microplates could be synthesized at the molar ratio of 9:1. A possible morphological formation mechanism of NaGd(MoO<sub>4</sub>)<sub>2</sub> tetragonal microplates was proposed, i.e. nucleation-Ostwald ripening growth process. Color tunable photoluminescence properties of NaGd(MoO<sub>4</sub>)<sub>2</sub>: Eu<sup>3+</sup>, Tb<sup>3+</sup> microcrystals were studied in detail. Among different morphologies of NaGd(MoO<sub>4</sub>)<sub>2</sub>: 5% Eu<sup>3+</sup> microcrystals, tetragonal microplates had a broadened, red-shifted and enhanced charge transfer band in the excitation spectrum. What's more, the full-width at half-maximum for the charge transfer band of the tetragonal plates was highest (58 nm), which favored efficient excitation and absorption in ultraviolet region. The introduction of a small amount of Tb<sup>3+</sup> into NaGd(MoO<sub>4</sub>)<sub>2</sub> microplates doped with Eu<sup>3+</sup> would enhance the <sup>5</sup>D<sub>0</sub>→<sup>7</sup>F<sub>J</sub> transition of Eu<sup>3+</sup> at 616 nm due to the energy transfer process of cross-relaxation from Tb<sup>3+</sup> to Eu<sup>3+</sup>. Multicolor tunable luminescence from deep red, red, orange, yellow to green under 291 nm ultraviolet excitation and from red, reddish orange to pink under 380 nm near-ultraviolet excitation could be obtained in NaGd(MoO<sub>4</sub>)<sub>2</sub> tetragonal microplates by simply adjusting the doping concentrations of Eu<sup>3+</sup> and Tb<sup>3+</sup>, suggesting NaGd(MoO<sub>4</sub>)<sub>2</sub>: Eu<sup>3+</sup>, Tb<sup>3+</sup> microcrystals might have practical application in optoelectronic devices, such as light emitting diodes and color display systems. This facile morphology-controlled hydrothermal synthesis strategy was simple, low-cost and environment-friendly, and might be extended to other inorganic materials.

### 1. Introduction

Lanthanide ions doped inorganic nano/microcrystals with well-defined morphology have attracted much attention due to their unique physicochemical properties and therefore potential applications in numerous fields such as light emitting diodes, color displays, bio-imaging, solar cell devices and photocatalysis.<sup>[1-5]</sup> As an important family of inorganic compounds, double alkaline rare-earth molybdates and tungstates have attracted much research attention because of their wide use as luminescent hosts, laser materials and

catalysts. Generally, double alkaline rare-earth molybdates share scheelite type (CaWO<sub>4</sub>) crystal structure with the nominal formula ARe(MoO<sub>4</sub>)<sub>2</sub> (where A = alkali metal cation, Re = trivalent rare-earth metal cation) and most of them have space group symmetry *I*4<sub>1</sub>/*a*.<sup>[6]</sup> Owing to their high chemical durability, large rare-earth ions admittance and large absorption cross-sections, double molybdate crystals have been studied in detail as laser host materials for decades.<sup>[7-10]</sup> Recently, many research efforts have been devoted to synthesis and luminescence properties of double molybdate nano/microcrystals. For example, Mo et al. synthesized NaGd(MO<sub>4</sub>)<sub>2</sub>:R (M = W, Mo, R = Eu<sup>3+</sup>, Sm<sup>3+</sup>, Bi<sup>3+</sup>) red-emitting phosphors by solid-state reaction method.<sup>[11]</sup> Katelnikovas et al. prepared Li<sub>3</sub>Ba<sub>2</sub>La<sub>3</sub>(MoO<sub>4</sub>)<sub>8</sub>:Eu<sup>3+</sup> powders and ceramics, and investigated their optical properties for light emitting diodes applications.<sup>[12]</sup> Wu et al. reported KEu(MoO<sub>4</sub>)<sub>2</sub> microcrystals with different morphologies synthesized via a molten salt method using halons as flux.<sup>[13]</sup> Krishnan et al. synthesized bipyramid (Na<sub>0.5</sub>Gd<sub>0.5</sub>)MoO<sub>4</sub>: Ln<sup>3+</sup> microcrystals by EDTA-aided

<sup>a</sup> State Key Laboratory of Optoelectronic Materials and Technologies, School of Physics and Engineering, Sun Yat-sen University, Guangzhou 510275, China. E-mail: stszyl@mail.sysu.edu.cn

<sup>b</sup> Institute of Optoelectronic Engineering, Jinan University, Guangzhou 510632, China

† Electronic Supplementary Information (ESI) available: Fig. S1-S7. See DOI: 10.1039/x0xx00000x

hydrothermal route, and investigated their up/down conversion luminescence, morphological formation mechanism and magnetic properties.<sup>[14]</sup> Xu et al. synthesized  $\text{NaEu}(\text{MoO}_4)_2$  with rugby-like microstructures and  $\text{NaY}(\text{MoO}_4)_2$  microcrystals with controllable morphologies via an EDTA-mediated hydrothermal method, and investigated their photoluminescence properties.<sup>[15, 16]</sup> Lin et al. reported flower-like  $\text{NaY}(\text{MoO}_4)_2$  microcrystals synthesized via hydrothermal method using polyvinylpyrrolidone as a template.<sup>[17]</sup> Jiang et al. synthesized  $\text{NaGd}(\text{MoO}_4)_2:\text{Eu}^{3+}/\text{Tb}^{3+}$  phosphors with octahedral morphology via a surfactant (glutamic acid) assisted hydrothermal method.<sup>[18]</sup> Generally, double molybdate nano/microcrystals were prepared by conventional solid-state reaction, molten salt synthesis or additives assisted hydrothermal method. Hydrothermal method based on aqueous-phase reaction at high pressures has a lower synthesis temperature and is morphology-controllable, compared with conventional synthesis technique, such as solid state reaction and molten salt synthesis. However, additives assisted hydrothermal synthesis method, using organic surfactants, organic solvents, capping agents, or templates as additives, has several disadvantages such as toxicity, high cost and difficulty in effective removal of additives. In contrast, additives-free hydrothermal synthesis method under mild conditions is simple, low-cost, and environment-friendly. To the best of our knowledge, facile additives-free and morphology-controllable hydrothermal synthesis of  $\text{NaGd}(\text{MoO}_4)_2$  microcrystals, as well as photoluminescence properties of tetragonal  $\text{NaGd}(\text{MoO}_4)_2$  plates, has not been reported before.

In this paper, we report a facile morphology-controllable hydrothermal synthesis of  $\text{NaGd}(\text{MoO}_4)_2$  microcrystals under mild conditions, and free of additives, such as organic surfactants and solvents, capping agents, or templates. By varying the molar ratios of  $\text{Na}_2\text{MoO}_4/\text{Gd}(\text{NO}_3)_3$  and pH values of the precursor solutions,  $\text{NaGd}(\text{MoO}_4)_2$  microcrystals with different morphologies, including bipyramids, truncated bipyramids, quasi-cubes and tetragonal plates, are synthesized successfully. A possible formation mechanism for tetragonal plate  $\text{NaGd}(\text{MoO}_4)_2$  microcrystals is proposed as well. Color tunable luminescence properties of  $\text{NaGd}(\text{MoO}_4)_2:\text{Eu}^{3+}, \text{Tb}^{3+}$  tetragonal microplates are also studied in detail.

## 2. Experimental section

### 2.1 Materials

The raw materials  $\text{Gd}_2\text{O}_3$  (99.99%),  $\text{Eu}_2\text{O}_3$  (99.99%),  $\text{Tb}_4\text{O}_7$  (99.99%) were purchased from Sun Chemical Technology Co. Ltd. (Shanghai, China), Sinopharm Chemical Reagent Co. Ltd. (Shanghai, China) and Aladdin Reagent Co. Ltd. (Shanghai, China) respectively. All other chemicals were of analytical grade. Sodium molybdate dihydrate ( $\text{Na}_2\text{MoO}_4 \cdot 2\text{H}_2\text{O}$ , 99%) was purchased from Tianjin Damao Chemical Reagent Factory (Tianjin, China).  $\text{HNO}_3$  and  $\text{NaOH}$  were purchased from Guangzhou Chemical Reagent Factory (Guangzhou, China). All

chemical reagents were used as received without any further purification. Deionized water was used throughout.

### 2.2 Synthesis

$\text{Gd}(\text{NO}_3)_3$  was prepared by dissolving appropriate amounts of  $\text{Gd}_2\text{O}_3$  in diluted nitric acid under vigorous stirring and heating in water bath. After the powders were all dissolved, the above solution was evaporated to dryness, and redissolved in appropriate amounts of deionized water to form  $\text{Gd}(\text{NO}_3)_3$  solution.  $\text{Eu}(\text{NO}_3)_3$  and  $\text{Tb}(\text{NO}_3)_3$  were prepared in the same procedure except for using  $\text{Eu}_2\text{O}_3$  and  $\text{Tb}_4\text{O}_7$  instead of  $\text{Gd}_2\text{O}_3$ , respectively.

In a typical synthesis procedure for undoped  $\text{NaGd}(\text{MoO}_4)_2$  microcrystals, a predetermined amount of  $\text{Na}_2\text{MoO}_4 \cdot 2\text{H}_2\text{O}$  was dissolved in 20 ml deionized water with strong magnetic stirring for 10 minutes to form aqueous solution. The above solution was added dropwise into  $\text{Gd}(\text{NO}_3)_3$  solution (1M) under vigorous stirring, and a white precipitate was obtained. The pH value of the obtained colloidal suspension was adjusted by adding diluted  $\text{HNO}_3$  or  $\text{NaOH}$  solution drop by drop. After additional agitation for 1h, the as-obtained colloidal suspension was transferred to a 60ml Teflon-lined stainless steel autoclave. Then the autoclave was sealed and maintained at 180 °C for 12h in an oven. After cooling down to room temperature, the final precipitate products were collected by centrifugation, washed several times with deionized water and ethanol, and dried at 60 °C for 5h in air.  $\text{NaGd}(\text{MoO}_4)_2:\text{Eu}^{3+}, \text{Tb}^{3+}$  microcrystals were synthesized in the same procedure except that a mixed solution of  $\text{Gd}(\text{NO}_3)_3$ ,  $\text{Eu}(\text{NO}_3)_3$  and/or  $\text{Tb}(\text{NO}_3)_3$  was used instead of  $\text{Gd}(\text{NO}_3)_3$  solution. Typical hydrothermal synthetic parameters were as follows,  $\text{Na}_2\text{MoO}_4/\text{Gd}(\text{NO}_3)_3$  molar ratios and pH values of the precursor solutions were 3:1 and 4.5 for bipyramids, 5:1 and 4.5 for truncated bipyramids, 6:1 and 5.0 for quasi-cubes, and 9:1 and 4.5 for tetragonal plates, respectively.

### 2.3 Characterization

Crystal structure and phase purity of the samples were examined by powder X-ray diffraction (XRD) performed on a Rigaku D-MAX 2200 VPC diffractometer with  $\text{Cu K}\alpha$  radiation ( $\lambda = 0.15405$  nm) at a scanning rate of 8°/min in a 2 theta range of 10–80°. Scanning electron microscope (SEM, JEOL JSM-6330F) and transmission electron microscope (TEM, JEOL JEM-2010HR) were employed for the observation of the morphology. Low-resolution TEM images, high-resolution TEM (HRTEM) images and selected-area electron diffraction (SAED) patterns were performed at an accelerating voltage of 200 kV. The photoluminescence excitation and emission spectra were recorded at room temperature on an Edinburgh FLSP920 spectrometer equipped with a Czerny-Turner monochromator, using a 450 W continuous xenon lamp as excitation source and a R928 red-sensitive photomultiplier tube as detector (excitation and emission slits were both set at a width of 0.5 mm).

## 3. Results and discussion

### 3.1 Crystal structure and morphology

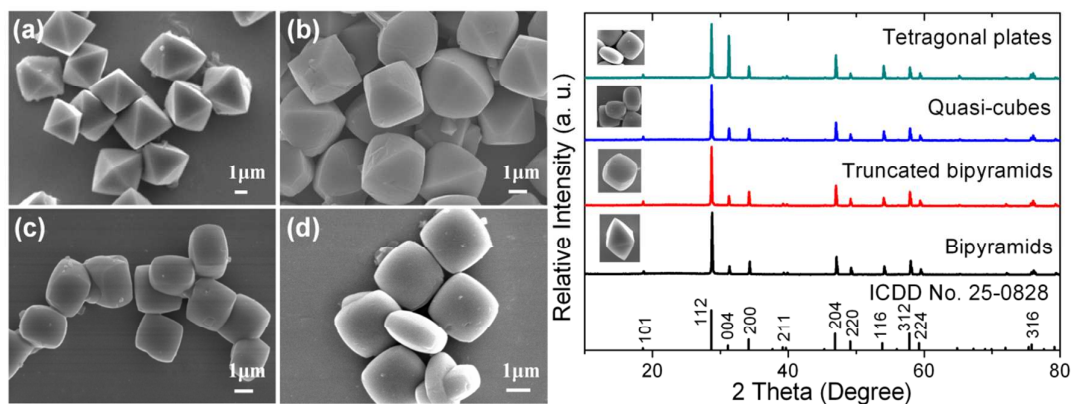


Fig. 1 SEM images of the synthesized  $\text{NaGd}(\text{MoO}_4)_2$  samples with different morphologies, i.e. (a) bipyramids, (b) truncated bipyramids, (c) quasi-cubes, (d) tetragonal plates. (e) XRD patterns of these samples and standard ICDD pattern (No. 25-0828).

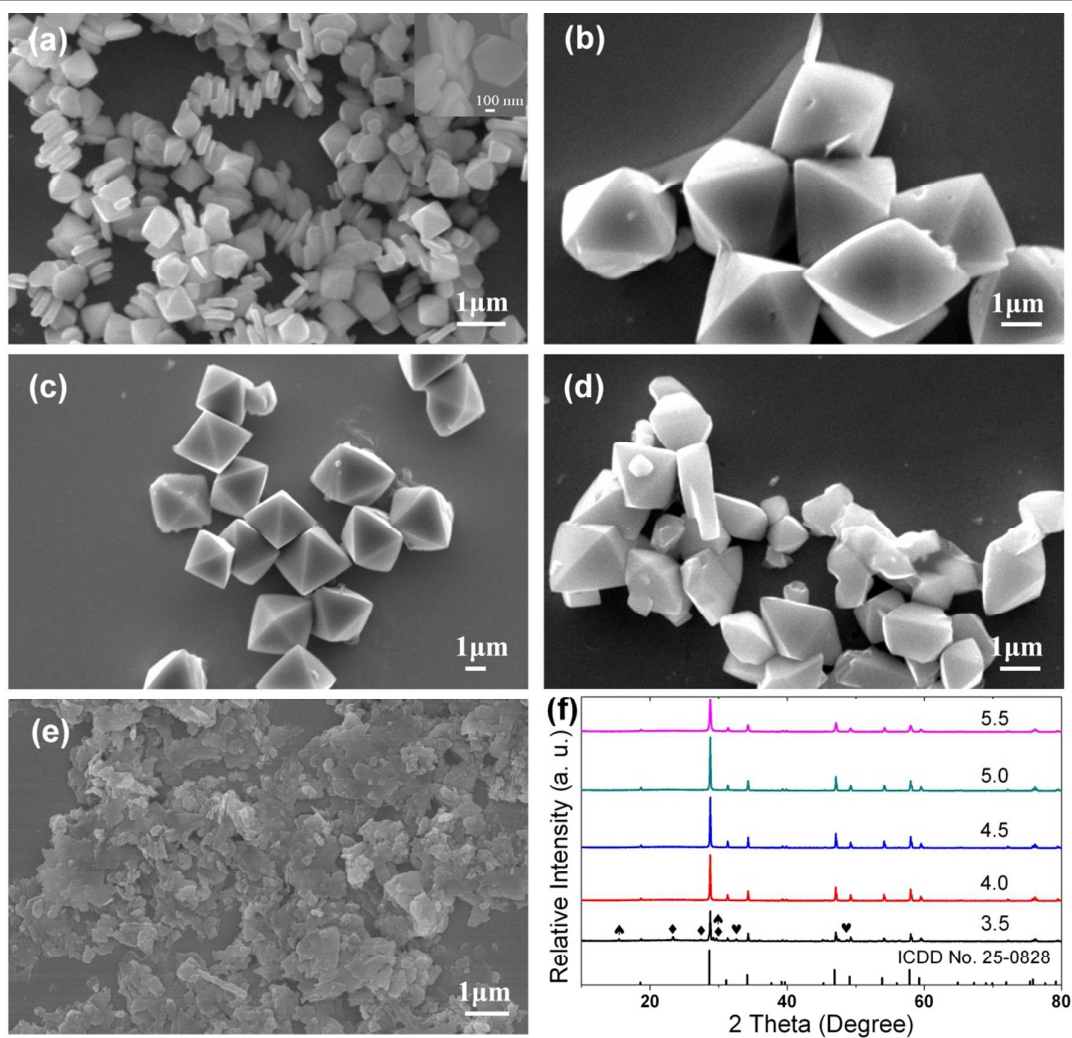


Fig. 2 SEM images of the  $\text{NaGd}(\text{MoO}_4)_2$  samples synthesized at  $\text{Na}_2\text{MoO}_4/\text{Gd}(\text{NO}_3)_3$  molar ratio of 3:1 and different pH values: (a) pH = 3.5, (b) pH = 4.0, (c) pH = 4.5, (d) pH = 5.0, (e) pH = 5.5. (f) XRD patterns of these samples and standard ICDD pattern (No. 25-0828). (Traces of  $\text{MoO}_3$  (ICDD No. 35-0609),  $\text{Gd}_2(\text{MoO}_4)_3$  (ICDD No. 26-0655) and  $\text{Gd}_2(\text{MoO}_4)_3$  (ICDD No. 24-0428) are marked by  $\blacklozenge$ ,  $\blacktriangle$  and  $\blacktriangledown$  respectively).

$\text{NaGd}(\text{MoO}_4)_2$  microcrystals with different morphologies are synthesized hydrothermally by varying the molar ratios of  $\text{Na}_2\text{MoO}_4/\text{Gd}(\text{NO}_3)_3$  and pH values of the initial precursor solutions at 180 °C for 12h. Crystal structures and morphologies of the as-prepared samples are characterized by powder XRD and SEM. Fig. 1 presents the SEM images and XRD patterns of the as-synthesized samples of  $\text{NaGd}(\text{MoO}_4)_2$  microcrystals with different morphologies. As can be seen obviously in the SEM images of Fig.1, the products are uniform and well-crystallized microcrystals with different morphologies including tetragonal plates, quasi-cubes, truncated bipyramids, and bipyramids. All the characteristic diffraction peaks in these XRD patterns of Fig. 1 match well with the tetragonal phase  $\text{NaGd}(\text{MoO}_4)_2$  with the space group  $I4_1/a$  (ICDD No. 25-0828) and no additional peaks or other phases can be found, indicating that the synthesized samples are single tetragonal phase  $\text{NaGd}(\text{MoO}_4)_2$  with the space group  $I4_1/a$ . The sharp and strong diffraction peaks indicate high crystallinity. In the XRD patterns of the tetragonal plates, the relative diffraction

intensity ratio of (004)/(101) increases significantly compared with the standard diffraction patterns, implying preferentially oriented crystallization along the (001) planes, which is in good agreement with the observed morphology. The TEM images, HRTEM images and SAED patterns of bipyramids and tetragonal plates are shown in Fig. S1 (ESI).

### 3.2 Effects of pH values and $\text{Na}_2\text{MoO}_4/\text{Gd}(\text{NO}_3)_3$ molar ratios on phase and morphology

A series of  $\text{NaGd}(\text{MoO}_4)_2$  microcrystals are synthesized by varying pH values and  $\text{Na}_2\text{MoO}_4/\text{Gd}(\text{NO}_3)_3$  molar ratios of the precursor solution, while synthesizing temperature and reaction time are 180 °C and 12h, respectively. The effects of the pH values and molar ratios on phase and morphology are systematically investigated.

Fig. 2 shows the SEM images and XRD patterns of the samples obtained at the  $\text{Na}_2\text{MoO}_4/\text{Gd}(\text{NO}_3)_3$  molar ratio of 3:1 and different pH values varying from 3.5 to 5.5. When the pH

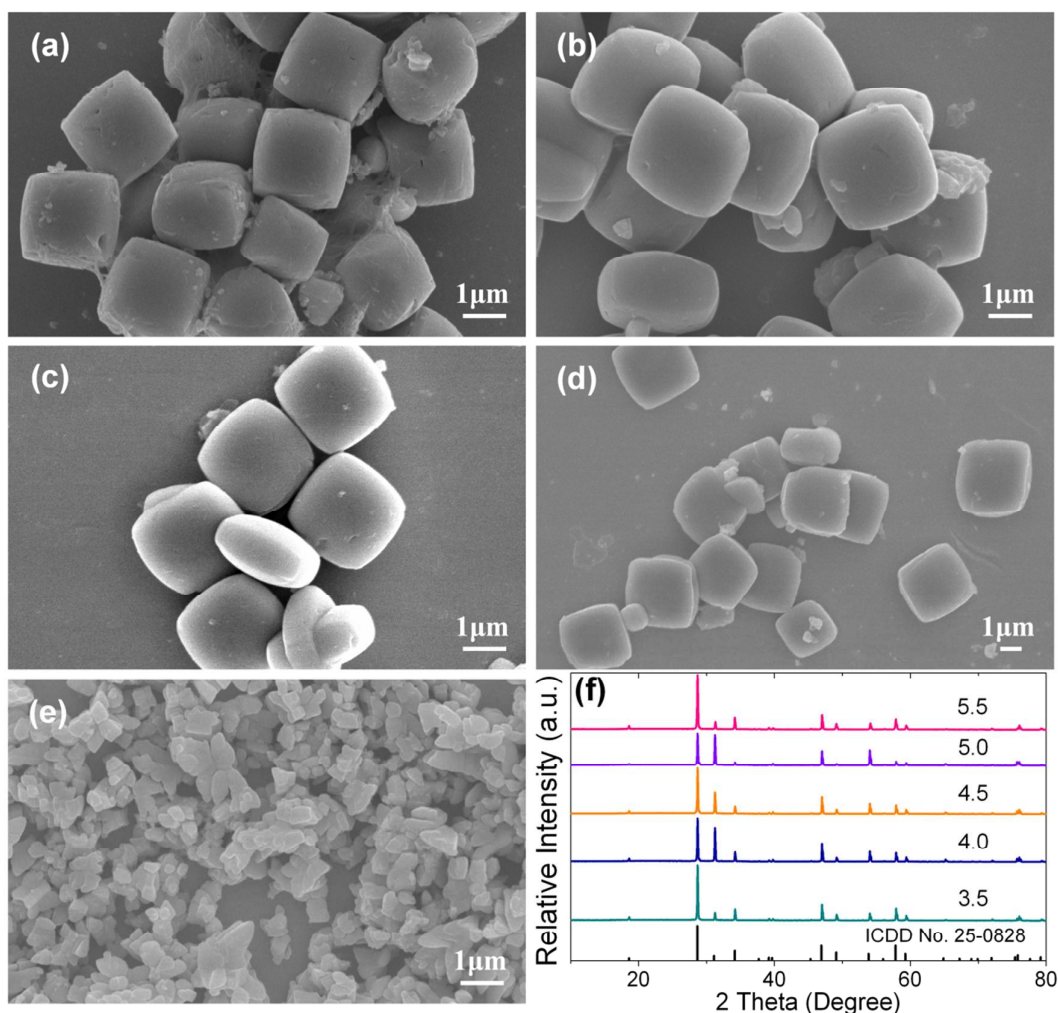


Fig. 3 SEM images of the  $\text{NaGd}(\text{MoO}_4)_2$  samples synthesized at  $\text{Na}_2\text{MoO}_4/\text{Gd}(\text{NO}_3)_3$  molar ratio of 9:1 and different pH values: (a) pH = 3.5, (b) pH = 4.0, (c) pH = 4.5, (d) pH = 5.0, (e) pH = 5.5. (f) XRD patterns of these samples and standard ICDD pattern (No. 25-0828).

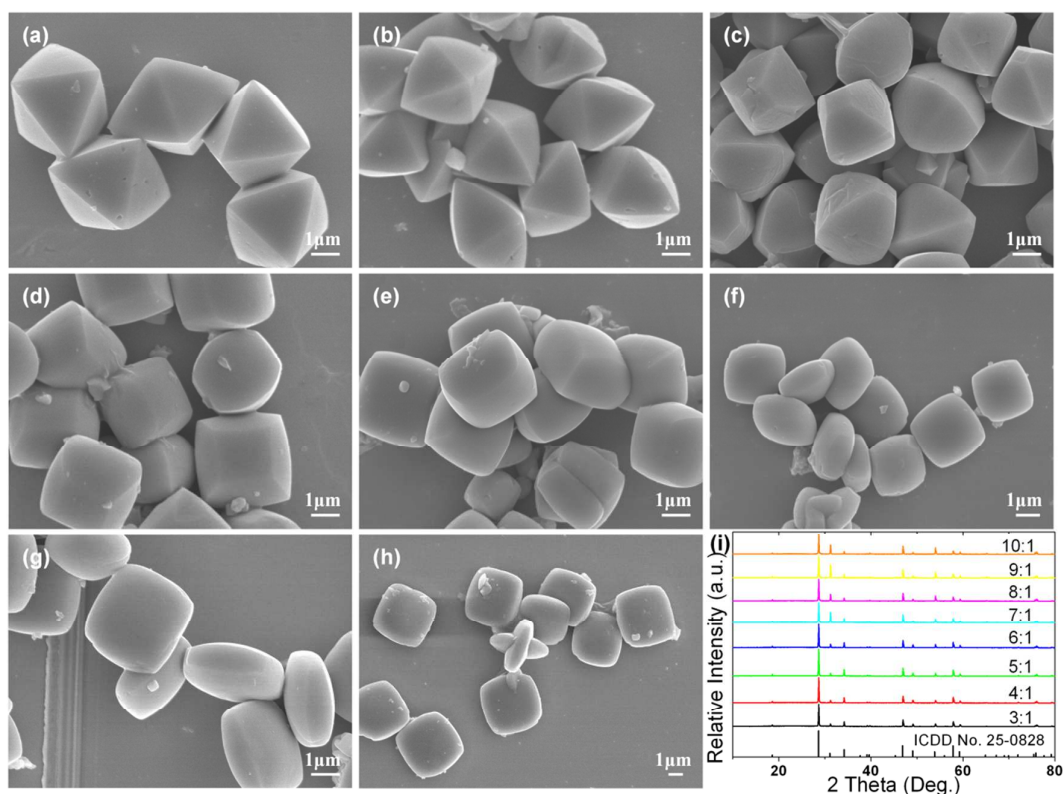


Fig. 4 SEM images of the  $\text{NaGd}(\text{MoO}_4)_2$  samples synthesized at pH values of 4.5 and different  $\text{Na}_2\text{MoO}_4/\text{Gd}(\text{NO}_3)_3$  molar ratios: (a) 3:1, (b) 4:1, (c) 5:1, (d) 6:1, (e) 7:1, (f) 8:1, (g) 9:1, (h) 10:1. (i) XRD patterns of these samples and standard ICDD pattern (No. 25-0828).

value is 3.5, the SEM image shows that the products exhibit the morphology of submicro-bipyramids and hexagonal nanoflakes, and the XRD pattern shows impurity peaks of  $\text{MoO}_3$  and  $\text{Gd}_2(\text{MoO}_4)_3$ . When the pH value is adjusted to 4.0 or 4.5, well-defined uniform bipyramid-like microcrystals with side length of about  $2 \mu\text{m}$  are observed in the SEM images. Meanwhile, pure tetragonal phase  $\text{NaGd}(\text{MoO}_4)_2$  without impurity phases are detected in the corresponding XRD patterns. Moreover, this tetragonal bipyramid-like morphology with 4-fold rotational symmetry is consistent with the symmetrical characteristic of space group  $I4_1/a$ . The morphology of the products become irregular at the pH value of 5.0, and when the pH value is 5.5 the products exhibit irregular sheet-like morphology. The products are pure tetragonal phase as the pH values are 5.0 and 5.5, though the peaks in the XRD pattern of samples synthesized at pH value of 5.5 are broad and weak.

Fig. 3 shows the SEM images and XRD patterns of the samples obtained at the  $\text{Na}_2\text{MoO}_4/\text{Gd}(\text{NO}_3)_3$  molar ratio of 9:1 and different pH values varying from 3.5 to 5.5. When the pH value is 3.5, quasi-cubes are observed. When the pH values increase from 4.0 to 5.0, the morphologies of the products are all uniformly dispersed tetragonal plates, of which the thickness decrease with the increasing pH values. Typically, the thickness and side length of the tetragonal microplates are 0.5 and  $2 \mu\text{m}$  at the pH value of 4.5. When the pH value is

increased to 5.5, the samples exhibit irregular sheets. Identified by XRD analysis, all these samples synthesized at molar ratio of 9:1 are pure tetragonal phase  $\text{NaGd}(\text{MoO}_4)_2$ . As is shown in Fig. 3, the diffraction intensity of (004) increases remarkably in the XRD patterns of the samples synthesized at pH values of 4.0, 4.5 and 5.0. The exposed tetragonal sections of the tetragonal plates present preferentially oriented crystallization along the (001) plane in the  $\text{NaGd}(\text{MoO}_4)_2$  microcrystals. A similar morphological variation along with increasing pH values is also found when the  $\text{Na}_2\text{MoO}_4/\text{Gd}(\text{NO}_3)_3$  molar ratio is 4:1, 6:1 or 8:1 (see Fig. S2, ESI). The XRD patterns of the products obtained at molar ratios of 4:1, 6:1 and 8:1 indicates that they are all pure phase  $\text{NaGd}(\text{MoO}_4)_2$  (see Fig. S3, ESI)

Fig. 4 presents the SEM images of the samples synthesized at pH values of 4.5 and different molar ratios varying from 3:1 to 10:1. When the molar ratio is 3:1 or 4:1, the SEM image shows uniform tetragonal bipyramids. When the molar ratio is 5:1 or 6:1, truncated bipyramids are obtained. What's more, morphological truncation degree increase with increasing  $\text{Na}_2\text{MoO}_4/\text{Gd}(\text{NO}_3)_3$  molar ratios. When the molar ratio is 7:1 or bigger, the morphologies of the samples exhibit tetragonal plates. The thickness of the plates decreases as the molar ratio increases.

From the above experimental results, it can be found that the pH values of the precursor solutions and the

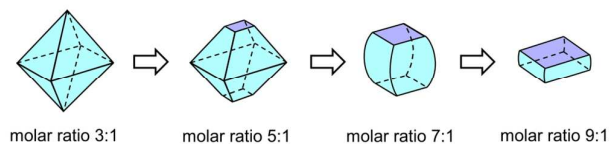


Fig. 5 Schematic illustration of morphological transformation with increasing  $\text{Na}_2\text{MoO}_4/\text{Gd}(\text{NO}_3)_3$  molar ratios at appropriate pH value.

$\text{Na}_2\text{MoO}_4/\text{Gd}(\text{NO}_3)_3$  molar ratios have combined effects in the synthesis of pure phase  $\text{NaGd}(\text{MoO}_4)_2$  microcrystals with specific regular morphology. The pH values play an important role in the formation of pure phase and regular morphology of the final products. Moreover, the  $\text{Na}_2\text{MoO}_4/\text{Gd}(\text{NO}_3)_3$  molar ratios play crucial role in the morphology-controllable synthesis of  $\text{NaGd}(\text{MoO}_4)_2$  microcrystals. For the case of tetragonal structure system, the surface energy of {001} facets is higher than {101} facets according to Donnay-Harker rules.<sup>[19]</sup> A faster growth rate along the direction perpendicular to the {001} planes with higher surface energy will lead to the formation of tetragonal bipyramid morphology enclosed by exposed {101} facets. The facets with higher surface energy will disappear and not be expressed in the final equilibrium morphology as a result of the minimization of total surface energy, according to Gibbs-Wulff theorem.<sup>[20, 21]</sup> Thus bipyramid  $\text{NaGd}(\text{MoO}_4)_2$  microcrystals can be synthesized at appropriate pH values under lower  $\text{Na}_2\text{MoO}_4/\text{Gd}(\text{NO}_3)_3$  molar ratio conditions. Higher or lower pH value would change the growth rate of crystallographic facets with different surface energies. Consequently, the nucleation and growth behavior would be out of kinetic control and the final products tend to be irregular and impure.<sup>[22]</sup> It is found that the precursor solution's pH value of about 4.5 will lead to regular and uniform morphology of products with pure phase and high crystallinity. With regard to the effects of molar ratios, higher  $\text{Na}_2\text{MoO}_4/\text{Gd}(\text{NO}_3)_3$  molar ratio will cause higher  $\text{MoO}_4^{2-}$  content. Due to electrostatic interaction, excess  $\text{MoO}_4^{2-}$  ions will preferentially adsorb on {001} planes, which have a higher packing density of  $\text{Na}^+$  and  $\text{Gd}^{3+}$  ions than other faces.<sup>[23]</sup> As a result, the reactivity and the growth rate of high-energy {001} facets will be reduced, and {001} facets will still remain in the final morphology. Therefore, under higher molar ratio conditions, there is a tendency to form tetragonal plates of which the thickness is reduced along with increasing molar ratios. On the basis of the above analyses, well-crystallized  $\text{NaGd}(\text{MoO}_4)_2$  microcrystals with different morphologies can be selectively synthesized by judicious choice of  $\text{Na}_2\text{MoO}_4/\text{Gd}(\text{NO}_3)_3$  molar ratios and pH values of the precursor solution.

### 3.3 Formation mechanism of $\text{NaGd}(\text{MoO}_4)_2$ micro crystals: tetragonal microplates as an example

As previously mentioned, different  $\text{Na}_2\text{MoO}_4/\text{Gd}(\text{NO}_3)_3$  molar ratios and pH values of the precursor solution will lead to different crystal morphologies of the products, which is the key to morphology-controllable synthesis of the  $\text{NaGd}(\text{MoO}_4)_2$

microcrystals. The growth of {001} facets will be inhibited when adsorbed by excess  $\text{MoO}_4^{2-}$  ions. At different molar ratios in an appropriate pH range, tetragonal bipyramids, truncated bipyramids, quasi-cubes and tetragonal plates are produced respectively. The morphologies of the products transform from bipyramids, truncated bipyramids, quasi-cubes to tetragonal plates with increasing  $\text{Na}_2\text{MoO}_4/\text{Gd}(\text{NO}_3)_3$  molar ratios at pH values of 4.5, as schematically shown in Fig. 5.

Since it's hard to track the growth of nano/microcrystals in solutions directly, the formation mechanisms are mostly elucidated by investigation of morphologies and crystal structures of the samples obtained at different reaction stages. In order to further reveal the formation mechanism of  $\text{NaGd}(\text{MoO}_4)_2$  microcrystals, time-dependent evolution experiments of tetragonal plates are conducted as an example. SEM images and XRD patterns of the samples synthesized at 180 °C, pH of 4.5 and molar ratio of 9:1 with different reaction time (0 h, 0.5 h, 1 h, 2 h, 6 h) are presented in Fig. 6.

Initially, when the reaction time is 0 h or 0.5 h, the XRD patterns of the products exhibit broad and weak peaks from  $\text{Gd}_2(\text{MoO}_4)_3$ ,  $\text{MoO}_3$  and  $\text{Na}_2\text{MoO}_4$ , which suggests that poor-crystalline intermediates are formed in the precursor solution at the beginning of hydrothermal reaction. The corresponding products exhibit round shape sheets and irregular sheets at reaction time of 0 and 0.5 h, as is shown in SEM images of Fig. 6. When the reaction time is 1 h, the diffraction peaks in the XRD patterns become sharper and stronger, and the peaks fit well with the pure tetragonal phase  $\text{NaGd}(\text{MoO}_4)_2$  (ICDD No. 25-0828), indicating that the intermediates are converted to  $\text{NaGd}(\text{MoO}_4)_2$ . Correspondingly, rudiments of tetragonal plates along with some small particles appear in the SEM image. These show the initial formation of pure phase  $\text{NaGd}(\text{MoO}_4)_2$  microcrystals. However, small particles vanish at reaction time of 2 h, leaving tetragonal plates with slightly incomplete edges. The XRD patterns and SEM images of the products obtained at the reaction time of 2 h or longer reveal that the pure phase microplates become more intact and uniform. Eventually, well-crystallized and pure phase  $\text{NaGd}(\text{MoO}_4)_2$  microplates are synthesized.

It is generally acknowledged that the kinetics and thermodynamics have comprehensive effects on the morphological formation of nano/microcrystals. For instance, the crystal size distribution is generally determined by the competition between nucleation and crystal growth rate, and the morphology evolution is mainly driven by the reduction in surface free energy. When the sodium molybdate is added into the gadolinium nitrate solution, white precipitation intermediates are formed as precursors. Then the precursors might be dissolved and converted to  $\text{NaGd}(\text{MoO}_4)_2$  nuclei gradually. A small amount of rudimental  $\text{NaGd}(\text{MoO}_4)_2$  tetragonal plates appears along with the proceeding hydrothermal reaction. Parts of the  $\text{NaGd}(\text{MoO}_4)_2$  nuclei grow up to rudimental plates which have a lower surface free energy than the nuclei. Then the large plates grow even bigger at the expense of smaller ones due to further reduction of surface free energy through Ostwald ripening. Finally, uniform microcrystals with the morphology of tetragonal plates are

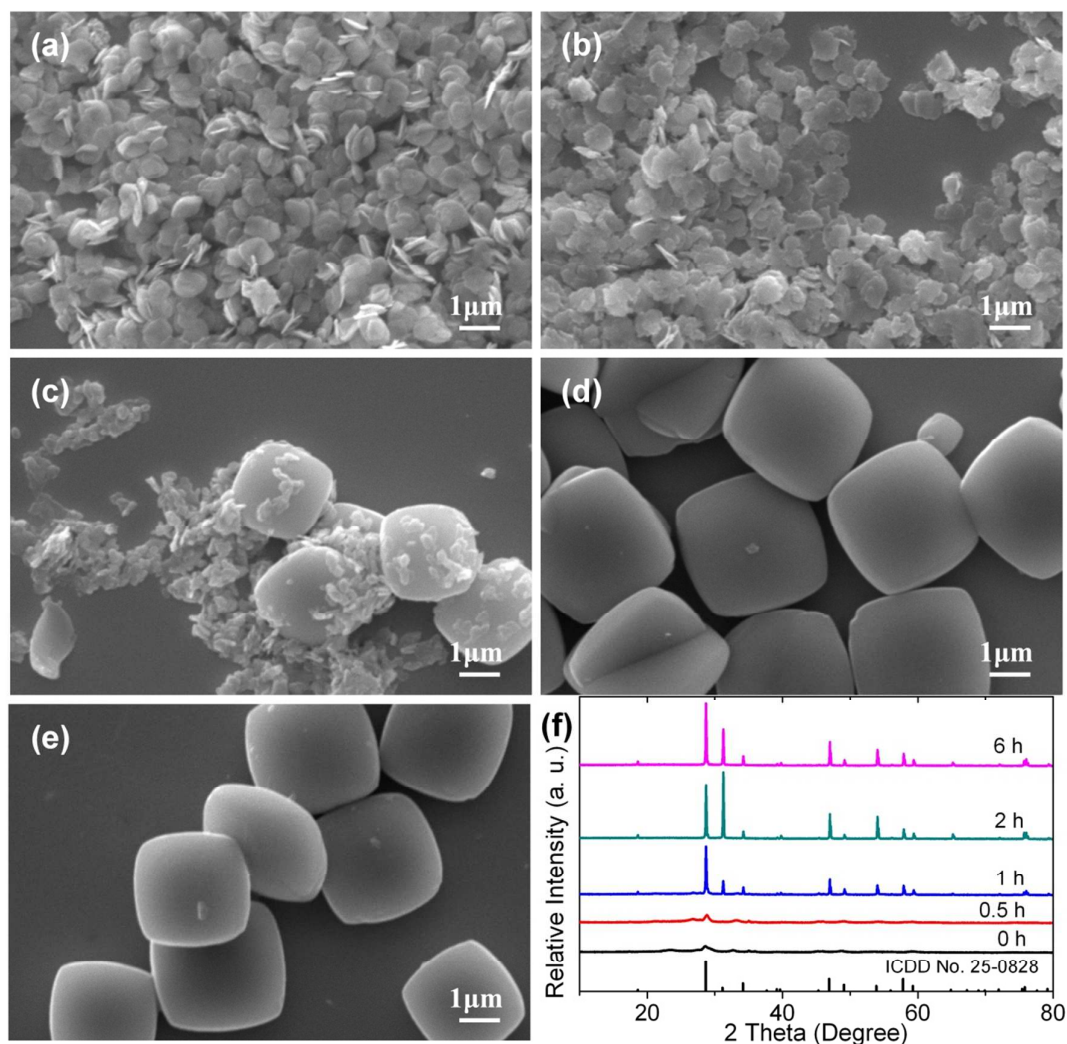


Fig. 6 SEM images of the  $\text{NaGd}(\text{MoO}_4)_2$  samples synthesized at  $180^\circ\text{C}$  and  $\text{pH} = 4.5$  with different reaction times: (a) 0 h, (b) 0.5 h, (c) 1 h, (d) 2 h, (e) 6 h. (f) XRD patterns of these samples and standard ICDD pattern (No. 25-0828).

formed. Based on the above analysis, the formation of  $\text{NaGd}(\text{MoO}_4)_2$  tetragonal microplates is believed to follow the nucleation-Ostwald ripening growth process, as is schematically shown in Fig. 7.3.4 Photoluminescence properties of  $\text{NaGd}(\text{MoO}_4)_2: \text{Eu}^{3+}, \text{Tb}^{3+}$

### 3.4.1 Photoluminescence properties of $\text{NaGd}(\text{MoO}_4)_2: 5\% \text{Eu}^{3+}$ with different morphologies.

Fig. 8 shows the photoluminescence excitation spectra of  $\text{NaGd}(\text{MoO}_4)_2: 5\% \text{Eu}^{3+}$  microcrystals with different morphologies, monitoring the red emission of  $\text{Eu}^{3+}$  at 616 nm. As is shown in Fig. 8, a broad excitation band from 250 to 350 nm is observed, which is attributed to the  $\text{O}^{2-}-\text{Mo}^{6+}$  charge transfer (C-T) absorption. The other sharp lines in the range from 360 nm to 550 nm are assigned to characteristic intra-configurational f-f transitions of  $\text{Eu}^{3+}$  ions, i.e.,  ${}^7\text{F}_0 \rightarrow {}^5\text{D}_1$  (535.5 nm),  ${}^7\text{F}_0 \rightarrow {}^5\text{D}_2$  (465.5 nm),  ${}^7\text{F}_0 \rightarrow {}^5\text{D}_3$  (416.5 nm),  ${}^7\text{F}_0 \rightarrow {}^5\text{L}_6$  (395 nm), and  ${}^7\text{F}_0 \rightarrow {}^5\text{D}_4$  (362.5 nm).

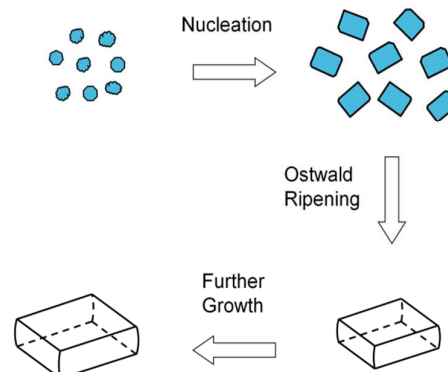


Fig. 7 Schematic illustration of the formation mechanism of  $\text{NaGd}(\text{MoO}_4)_2$  microplates.

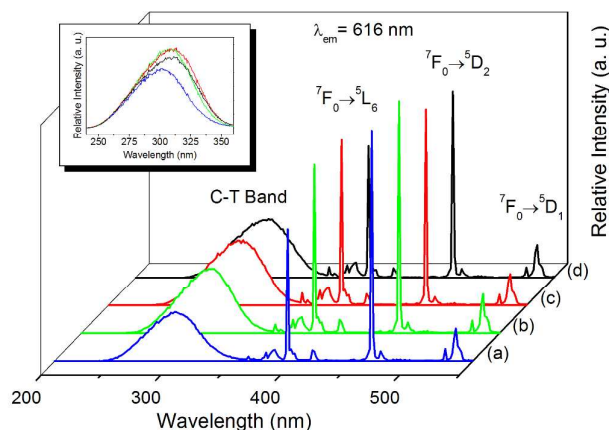


Fig. 8 Excitation spectra of  $\text{NaGd}(\text{MoO}_4)_2$ : 5%  $\text{Eu}^{3+}$  microcrystals with different morphologies: (a) bipyramids, (b) truncated bipyramids, (c) quasi-cubes, (d) tetragonal plates. The inset is partial excitation spectra of C-T band.

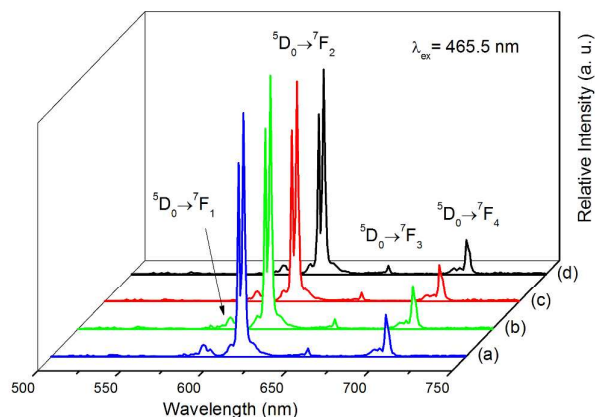


Fig. 9 Emission spectra of  $\text{NaGd}(\text{MoO}_4)_2$ : 5%  $\text{Eu}^{3+}$  microcrystals with different morphologies: (a) bipyramids, (b) truncated bipyramids, (c) quasi-cubes, (d) tetragonal plates.

Fig. 9 shows the photoluminescence emission spectra of  $\text{NaGd}(\text{MoO}_4)_2$ : 5%  $\text{Eu}^{3+}$  microcrystals with different morphologies under 465.5 nm excitation. The emission spectra consists of several  ${}^5\text{D}_0 \rightarrow {}^7\text{F}_J$  ( $J = 1, 2, 3, 4$ ) emission lines of  $\text{Eu}^{3+}$  at 592, 616, 655 and 702 nm, with the strongest emission at 616 nm for  $J=2$ . The emission peak at 616 nm is observed to split into two sub-peaks due to the Stark energy splitting.  $\text{Eu}^{3+}$  ions are universally known as structure probes to investigate the local environment in crystal. If the electric dipole transition  ${}^5\text{D}_0 \rightarrow {}^7\text{F}_2$  is dominant, the  $\text{Eu}^{3+}$  ions occupy sites without inversion symmetry; however, when the magnetic dipole transition  ${}^5\text{D}_0 \rightarrow {}^7\text{F}_1$  is dominant, the  $\text{Eu}^{3+}$  ions are in the sites of inversion center. In our case, the emission peak at 616 nm, which is contributed to  ${}^5\text{D}_0 \rightarrow {}^7\text{F}_2$  transition, is stronger than other peaks, indicating that  $\text{Eu}^{3+}$  ions occupy the asymmetry sites. Furthermore, the predominant emission peak at 616 nm is favorable to the high purity of red color.

Among different morphologies of  $\text{NaGd}(\text{MoO}_4)_2$ : 5%  $\text{Eu}^{3+}$  microcrystals (i.e. bipyramids, truncated bipyramids, quasi-cubes and tetragonal plates), their C-T bands in photoluminescence excitation spectra have a significant difference as is shown in the inset of Fig. 8. The C-T band of tetragonal microplates broadens, its peak shifts to long-wavelength direction and its intensity increases, compared to that of bipyramids (the peak of C-T band is located at 302 nm for bipyramids, and 311.5 nm for microplates). The full-width at half-maximum (FWHM) for the C-T band of tetragonal plates is about 58 nm, which is the highest among different morphologies (the FWHM is 49, 51 and 55 nm for the C-T band of bipyramids, truncated bipyramids and quasi-cubes, respectively). A broadened, red-shifted and enhanced charge transfer band in the excitation spectra favors efficient excitation and absorption in ultraviolet (UV) region for various optoelectronic device applications.

**3.4.2 Color tunable photoluminescence properties of  $\text{NaGd}(\text{MoO}_4)_2$ :  $\text{Eu}^{3+}$ ,  $\text{Tb}^{3+}$  tetragonal microplates.** Fig. S4 (ESI) shows the photoluminescence excitation and emission spectra of  $\text{NaGd}(\text{MoO}_4)_2$ : 5%  $\text{Tb}^{3+}$  tetragonal plates. The excitation spectrum obtained by monitoring the green emission of  $\text{Tb}^{3+}$  ions at 544 nm reveals a broad excitation band (with maximum at 291 nm) from 250 to 350 nm and a sharp absorption peak at 486.5 nm. The former (broad band) is ascribed to the C-T transition between  $\text{Mo}^{6+}$  and  $\text{O}^{2-}$  and the latter (peak centered at 486.5 nm) is assigned to the  ${}^7\text{F}_6 \rightarrow {}^5\text{D}_4$  transition of  $\text{Tb}^{3+}$  ions. The emission spectrum under 291 nm excitation exhibits several emission peaks at 489, 544, 588 and 622 nm assigned to the characteristic  ${}^5\text{D}_4 \rightarrow {}^7\text{F}_J$  ( $J = 3-6$ ) transitions of  $\text{Tb}^{3+}$  ions. The green emission at 544 nm ( ${}^5\text{D}_4 \rightarrow {}^7\text{F}_5$  transition of  $\text{Tb}^{3+}$ ) is the strongest among the transition emissions.

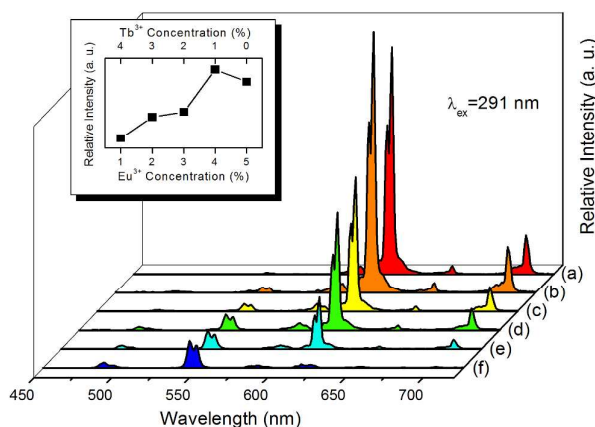


Fig. 10 Emission spectra of  $\text{NaGd}(\text{MoO}_4)_2$ :  $\text{Eu}^{3+}$ ,  $\text{Tb}^{3+}$  microplates with different doping concentrations excited at 291 nm: (a) 5%  $\text{Eu}^{3+}$ , (b) 4%  $\text{Eu}^{3+}$ , 1%  $\text{Tb}^{3+}$ , (c) 3%  $\text{Eu}^{3+}$ , 2%  $\text{Tb}^{3+}$ , (d) 2%  $\text{Eu}^{3+}$ , 3%  $\text{Tb}^{3+}$ , (e) 1%  $\text{Eu}^{3+}$ , 4%  $\text{Tb}^{3+}$ , (f) 5%  $\text{Tb}^{3+}$ . The inset is the relative intensities of red emission (616 nm) with different concentrations of  $\text{Eu}^{3+}$  and  $\text{Tb}^{3+}$  ions.

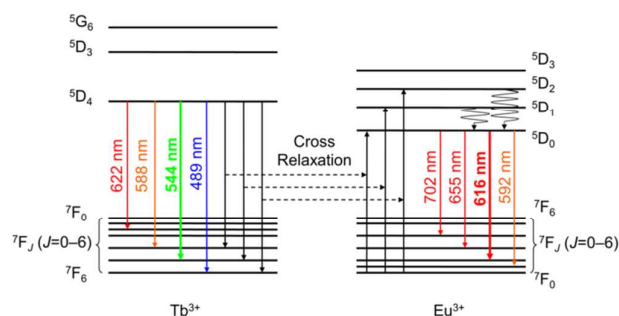


Fig. 11 Energy level scheme of energy transfer and radiative transition process of  $\text{Tb}^{3+}$  and  $\text{Eu}^{3+}$ .

The emission spectra of  $\text{NaGd}(\text{MoO}_4)_2: \text{Eu}^{3+}, \text{Tb}^{3+}$  tetragonal plates excited by 291 nm are depicted in Fig. 10. It is observed that the emission intensity at 544 nm increases gradually with increasing  $\text{Tb}^{3+}$  concentrations, and the red emission intensity at 616 nm increases with increasing  $\text{Eu}^{3+}$  concentrations. While the relative intensity of red emission at 616 nm reaches a maximum in  $\text{NaGd}(\text{MoO}_4)_2: 4\% \text{Eu}^{3+}, 1\% \text{Tb}^{3+}$ , then decreases with further increasing  $\text{Eu}^{3+}$  concentrations (or decreasing  $\text{Tb}^{3+}$  concentrations), as can be seen in the inset of Fig. 10. This may be the result of energy transfer from  $\text{Tb}^{3+}$  to  $\text{Eu}^{3+}$  ions. As is shown in Fig. S5 (ESI), there are overlaps between the emission spectrum of  $\text{NaGd}(\text{MoO}_4)_2: \text{Tb}^{3+}$  and the excitation spectrum of  $\text{NaGd}(\text{MoO}_4)_2: \text{Eu}^{3+}$ , implying a possible energy transfer from  $\text{Tb}^{3+}$  to  $\text{Eu}^{3+}$  ions.<sup>[24]</sup> As is shown in Fig. S6 (ESI), in the excitation spectrum of  $\text{NaGd}(\text{MoO}_4)_2: 1\% \text{Eu}^{3+}, 4\% \text{Tb}^{3+}$  monitoring the red emission of  $\text{Eu}^{3+}$  at 616 nm, an excitation peak of  $\text{Tb}^{3+}$  at 486.5 nm is observed. And the emission spectrum of  $\text{NaGd}(\text{MoO}_4)_2: 1\% \text{Eu}^{3+}, 4\% \text{Tb}^{3+}$  under excitation of 486.5 nm ( $\text{Tb}^{3+}$  characteristic absorption peak) exhibits characteristic emission peak of  $\text{Eu}^{3+}$  ions at 616 nm ( $^5\text{D}_0 \rightarrow ^7\text{F}_4$ ). All these evidences point to the energy transfer process from  $\text{Tb}^{3+}$  to  $\text{Eu}^{3+}$ , which has been observed in various hosts, such as  $\text{NaGd}(\text{MoO}_4)_2$  phosphors,  $\text{KLa}(\text{MoO}_4)_2$  microcrystals,  $\text{CaCO}_3$  phosphors, and  $\text{Y}_2\text{O}_3$  nanorods.<sup>[18, 25-27]</sup> So it is speculated that there exists an energy transfer process from  $\text{Tb}^{3+}$  to  $\text{Eu}^{3+}$  ions in  $\text{NaGd}(\text{MoO}_4)_2$  microplates. When a small amount of  $\text{Tb}^{3+}$  ions is introduced to  $\text{NaGd}(\text{MoO}_4)_2$  microplates doped with  $\text{Eu}^{3+}$  ions, the cross-relaxation of  $\text{Tb}^{3+} (^5\text{D}_4) + \text{Eu}^{3+} (^7\text{F}_0) \rightarrow \text{Tb}^{3+} (^7\text{F}_{4,5,6}) + \text{Eu}^{3+} (^5\text{D}_{0,1,2})$  and thereafter non-radiative multiphonon relaxation from the state  $^5\text{D}_{1,2}$  to  $^5\text{D}_0$  of  $\text{Eu}^{3+}$  ions will enhance the  $\text{Eu}^{3+} ^5\text{D}_0 \rightarrow ^7\text{F}_j$  radiative transitions, in which the red emission of  $^5\text{D}_0 \rightarrow ^7\text{F}_2$  is dominated (see Fig. 11 energy level scheme).<sup>[27]</sup> So the red emission intensity in the sample doped with 4%  $\text{Eu}^{3+}$  and 1%  $\text{Tb}^{3+}$  is stronger than that in the sample doped with 5%  $\text{Eu}^{3+}$ . The emission intensity of 616 nm in 5%  $\text{Eu}^{3+}$  doped sample is higher than that of 544 nm in 5%  $\text{Tb}^{3+}$  doped sample, suggesting higher luminescent efficiency of  $\text{Eu}^{3+}$  than that of  $\text{Tb}^{3+}$  in  $\text{NaGd}(\text{MoO}_4)_2$  hosts under 291 nm excitation of C-T band. There is a similar phenomenon in the emission spectra of  $\text{NaGd}(\text{MoO}_4)_2: \text{Eu}^{3+}$ ,

$\text{Tb}^{3+}$  under 380 nm near-UV excitation, as is shown in Fig. S7 (ESI).

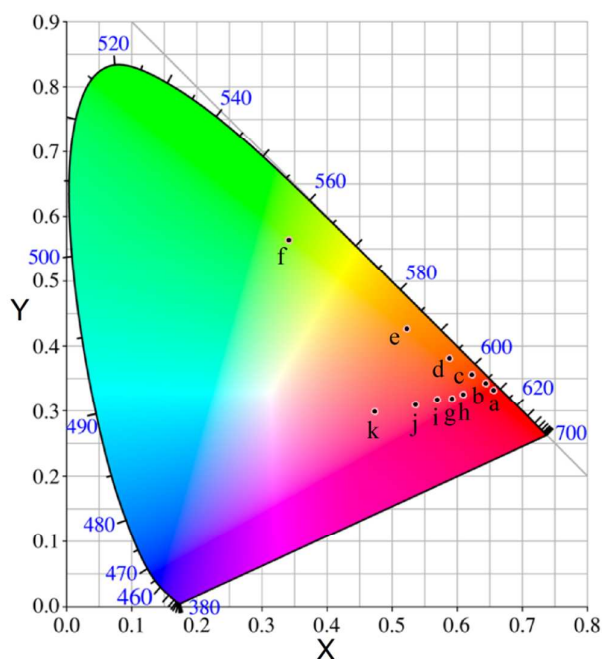


Fig. 12 CIE chromaticity diagram of  $\text{NaGd}(\text{MoO}_4)_2: \text{Eu}^{3+}, \text{Tb}^{3+}$  microplates with different doping concentrations excited at 291 nm (a. 5%  $\text{Eu}^{3+}$ ; b. 4%  $\text{Eu}^{3+}, 1\% \text{Tb}^{3+}$ ; c. 3%  $\text{Eu}^{3+}, 2\% \text{Tb}^{3+}$ ; d. 2%  $\text{Eu}^{3+}, 3\% \text{Tb}^{3+}$ ; e. 1%  $\text{Eu}^{3+}, 4\% \text{Tb}^{3+}$ ; f. 5%  $\text{Tb}^{3+}$ ) and 380 nm (g. 5%  $\text{Eu}^{3+}$ ; h. 4%  $\text{Eu}^{3+}, 1\% \text{Tb}^{3+}$ ; i. 3%  $\text{Eu}^{3+}, 2\% \text{Tb}^{3+}$ ; j. 2%  $\text{Eu}^{3+}, 3\% \text{Tb}^{3+}$ ; k. 1%  $\text{Eu}^{3+}, 4\% \text{Tb}^{3+}$ ).

Fig. 12 shows the Commission Internationale de l'éclairage (CIE, or International Commission on Illumination in English) chromaticity diagram of the emission spectra of  $\text{NaGd}(\text{MoO}_4)_2: \text{Eu}^{3+}, \text{Tb}^{3+}$  microcrystals with different concentrations. The chromaticity coordinates shift from deep red ( $x = 0.656, y = 0.333$ ) to green ( $x = 0.341, y = 0.565$ ) with the increasing  $\text{Tb}^{3+}$  or decreasing  $\text{Eu}^{3+}$  under UV excitation of 291 nm. When excited at near-UV 380 nm, the chromaticity coordinates shift from red ( $x = 0.609, y = 0.325$ ) to pink ( $x = 0.474, y = 0.298$ ). Thus a series of visible emission colors, such as red, orange, yellow, green and pink can be tuned efficiently by adjusting the doping concentration of  $\text{Eu}^{3+}$  and  $\text{Tb}^{3+}$  ions in  $\text{NaGd}(\text{MoO}_4)_2$  microcrystals under 291 nm UV excitation or 380 nm near-UV excitation.

#### 4. Conclusions

In conclusion, well-crystallized  $\text{NaGd}(\text{MoO}_4)_2$  microcrystals with the morphologies of bipyramids, truncated bipyramids, quasi-cubes and tetragonal plates are successfully synthesized via a facile additives-free hydrothermal synthesis method. The molar ratios of  $\text{Na}_2\text{MoO}_4/\text{Gd}(\text{NO}_3)_3$  and pH values of the precursor solutions play key roles in the selective synthesis of  $\text{NaGd}(\text{MoO}_4)_2$  microcrystals with different morphologies. A pH value of 4.5 is suitable for forming pure and regular

morphology of the final products. The morphological truncation degree of the obtained NaGd(MoO<sub>4</sub>)<sub>2</sub> microcrystals increases with increasing Na<sub>2</sub>MoO<sub>4</sub>/Gd(NO<sub>3</sub>)<sub>3</sub> molar ratios. Well-crystallized and uniform NaGd(MoO<sub>4</sub>)<sub>2</sub> tetragonal microplates are synthesized at molar ratio of 9:1 and pH value of 4.5. A possible formation mechanism of nucleation-Ostwald ripening is proposed to explain the formation and growth of NaGd(MoO<sub>4</sub>)<sub>2</sub> tetragonal microplates. This facile morphology-controlled synthesis strategy may be extended to other inorganic materials.

C-T band in the excitation spectrum of tetragonal microplates is broadened, red-shifted and has a highest full-width at half-maximum (58 nm) among different morphologies, which favors efficient excitation and absorption in ultraviolet region for various optoelectronic device applications. The introduction of a small amount of Tb<sup>3+</sup> ions into NaGd(MoO<sub>4</sub>)<sub>2</sub> microplates doped with Eu<sup>3+</sup> will enhance the <sup>5</sup>D<sub>0</sub>→<sup>7</sup>F<sub>J</sub> transitions of Eu<sup>3+</sup> at 616 nm due to the energy transfer process of cross-relaxation from Tb<sup>3+</sup> to Eu<sup>3+</sup>. As is confirmed by CIE chromaticity diagram, multicolor photoluminescence can be tuned efficiently in NaGd(MoO<sub>4</sub>)<sub>2</sub> microplates from deep red, orange, yellow to green under 291 nm UV excitation and from red, reddish orange to pink under 380 nm near-UV excitation, by simply adjusting the doping concentration of Eu<sup>3+</sup> and Tb<sup>3+</sup>. These results suggest that NaGd(MoO<sub>4</sub>)<sub>2</sub>: Eu<sup>3+</sup>, Tb<sup>3+</sup> microcrystals may have practical applications in various optoelectronic devices, such as light emitting diodes and color display systems.

## Acknowledgements

This work was supported by the National Natural Science Foundation of China under Grant No. 61176010 and No. 61172027, Guangdong Natural Science Foundation under Grant No. 2014A030311049, and the Research Foundation of IARC-SYSU under Grant No. IARC 2014-09.

## References

- 1 M. Haase and H. Schäfer, *Angew. Chem. Int. Ed.*, 2011, **50**, 5808-5829.
- 2 S. Ye, F. Xiao, Y. X. Pan, Y. Y. Ma and Q. Y. Zhang, *Mater. Sci. Eng., R*, 2010, **71**, 1-34.
- 3 S. V. Eliseeva and J. C. G. Bünzli, *New J. Chem.*, 2011, **35**, 1165-1176.
- 4 H. Q. Wang, M. Batentschuk, A. Osvet, L. Pinna, and C. J. Brabec, *Adv. Mater.*, 2011, **23**, 2675-2680.
- 5 A. Kudo and H. Kato, *Chem. Phys. Lett.*, 2000, **331**, 373-377.
- 6 G. Benoit, J. Véronique, A. Arnaud and G. Alain, *Solid State Sci.*, 2011, **13**, 460-467.
- 7 S. B. Stevens, C. A. Morrison, T. H. Allik, A. L. Rheingold, and B. S. Haggerty, *Phys. Rev. B*, 1991, **43**, 7386-7394.
- 8 J. M. Cano-Torres, M. D. Serrano, C. Zaldo, M. Rico, X. Mateos, J. Liu, U. Griebner, V. Petrov, F. J. Valle, M. Galan, and G. Viera, *J. Opt. Soc. Am. B*, 2006, **23**, 2494-2502.
- 9 X. Han, F. Fusari, M. D. Serrano, A. A. Lagatsky, J. M. Cano-Torres, C. T. A. Brown, C. Zaldo, and W. Sibbett, *Opt. Express*, 2010, **18**, 5413-5419.
- 10 J. Tang, Y. Chen, Y. Lin, X. Gong, J. Huang, Z. Luo, and Y. Huang, *Opt. Mater. Express*, 2012, **2**, 1064-1075.
- 11 F. Mo, L. Zhou, Q. Pang, F. Gong and Z. Liang, *Ceram. Int.*, 2012, **38**, 6289-6294.
- 12 A. Katelnikovas, J. Plewa, S. Sakirzanovas, D. Dutczak, D. Enseling, F. Baur, H. Winkler, A. Kareiva and T. Jüstel, *J. Mater. Chem.*, 2012, **22**, 22126-22134.
- 13 T. Wu, Y. Liu, Y. Lu, L. Wei, H. Gao and H. Chen, *CrystEngComm*, 2013, **15**, 2761-2768.
- 14 R. Krishnan and J. Thirumalai, *New J. Chem.*, 2014, **38**, 3480-3491.
- 15 L. Xu, X. Yang, Z. Zhai, X. Chao, Z. Zhang and W. Hou, *CrystEngComm*, 2011, **13**, 4921-4929.
- 16 L. Xu, X. Yang, H. Lu, C. Hu and W. Hou, *RSC Adv.*, 2014, **4**, 13502-13508.
- 17 H. Lin, X. Yan, X. Wang, *J. Solid State Chem.*, 2013, **204**, 266-271.
- 18 Y. Jiang, Y. Liu, G. Liu, X. Dong, J. Wang, W. Yu, Q. Dong, *Opt. Mater.* **36**, 1865-1870.
- 19 J. D. H. Donnay and D. Harker, *AM. Mineral.*, 1937, **22**, 446-467.
- 20 G. Wulff, *Z. Kristallogr.*, 1901, **34**: 449-530.
- 21 T. K. Sau and A. L. Rogach, *Adv. Mater.*, 2010, **22**, 1781-1804.
- 22 X. Sun and Y. Li, *Chem. Commun.*, 2003, **14**, 1768-1769.
- 23 S. Liu, D. Yang, D. Ma, S. Wang, T. Tang and S. Huang, *Chem. Commun.*, 2011, **47**, 8013-8015.
- 24 V. Naresh and S. Buddhudu, *J. Lumin.*, 2013, **137**, 15-21.
- 25 L. Hou, S. Cui, Z. Fu, Z. Wu, X. Fu and J. H. Jeong, *Dalton Trans.*, 2014, **43**, 5382-5392.
- 26 Q. Cheng, Y. Dong, M. Kang and P. Zhang, *J. J. Lumin.*, **156**, 91-96.
- 27 Z. Liu, L. Yu, Q. Wang, Y. Tao and H. Yang, *J. Lumin.*, 2011, **131**, 12-16.